ELSEVIER

International Journal of Solids and Structures 41 (2004) 5071–5085

INTERNATIONAL JOURNAL OF SOLIDS and STRUCTURES

www.elsevier.com/locate/ijsolstr

Modeling thin films applying an extended continuum theory based on a scalar-valued order parameter. Part I: isothermal case

Holger Steeb *, Stefan Diebels

Applied Mechanics, Saarland University, Im Stadtwald, Building 22, 66 123 Saarbrücken, Germany

Received 9 December 2003; received in revised form 17 March 2004
Available online 14 May 2004

Abstract

In the current work we develop a thermo-mechanically consistent model describing the behavior of thin polymeric films. In industrial applications of such thin films, e.g. in bonding metal sheets in automotive industry, boundary layers and, as a further result, scale effects depending on the thickness of the film are observed (see e.g. [Toney et al., 1995; Frank et al., 1996; J. Polym. Sci., Part B: Polym. Phys. 40 (2001) 2343–2353]). In contrast to the well-analyzed size effects in many other micro-structured materials, e.g. granular materials, porous materials or foams (see e.g. [Int. J. Mech. Sci. 43 (2001) 701–713] or [Proc. R. Soc. London A 458 (2002) 2869–2883]), the macroscopic behavior of the former material differs completely from an experimental point of view. In the analyzed polymeric films a weaker zone at the boundary of the film is observed in comparison with the stiffer material behavior of the bulk material. To capture these and more general types of boundary layer effects, we develop an extended continuum model based on a scalar-valued order parameter following the line of [Continua with Microstructures. Vol. 35 of Springer Tracts in Natural Philosophy. Springer, New York, 1980; Meccanica 17 (1982) 80–84; Ann. Mater. Pura Appl. 135 (1983) 1–25; Continuum Mech. Thermodyn. 4 (1999) 247–262].

PACS: 46.05.+b
Keywords: Extended continua; Thin films; Order parameter; Boundary layer

1. Introduction

The development of (macroscopic) continuum mechanical models for materials with microstructure traces back to the outstanding monograph on micropolar elasticity of the Cosserat brothers Eugène and François at the beginning of the last century, (see Cosserat and Cosserat, 1909). As this work was forgotten

* Corresponding author. Tel.: +49-6813022157; fax: +49-6813023992.
E-mail address: h.steeb@mx.uni-saarland.de (H. Steeb).
URL: http://www.uni-saarland.de/fak8/tm/.

0020-7683/$ - see front matter © 2004 Elsevier Ltd. All rights reserved.
doi:10.1016/j.ijsolstr.2004.03.013

for more than 40 years kinematically extended continuum models had a great revival in the mid fifties of the last century, (see e.g. the works of Günther, 1958; Mindlin and Tiersten, 1962; Eringen and Suhubi, 1964) and many others. [1] From a general point of view, all these theories are based on extended kinematic fields by introducing a priori additional degrees of freedom with independent motion functions for the material points of the microstructure. The additional motion functions are called micromotion in order to distinguish them from the classical motion function. As standard in rational continuum-thermodynamics (see e.g. the development in the classical work of Truesdell and Toupin (1960) or in the modern textbook of Šilhavý (1997)), the kinematical quantities, i.e. the micro- and macromotion have to be defined. This results in the question what the motion function for the special material with inherent microstructure is like. For *some* materials, again we mention open-cell foams or granular materials, this question can be answered in a satisfactory way, and in these special cases the micromotion is restricted to an orthogonal tensor (micropolar or Cosserat continuum) or an affine transformation (micromorphic continuum), e.g. Capriz (1980), Eringen (1999) and Diebels and Steeb (2002).

It was the effort of Capriz (1980), who has given a more general framework for the formulation of continua with arbitrary microstructure postulating an extended balance equation for the total energy. Thus, applying the concept of objectivity (frame indifference) vector valued higher order balance equations are obtainable naturally. In our investigation we restrict ourselves to scalar-valued order parameters which is comparable to the work of Svendsen (1999). In this special (invariant) case the higher order balance equation of the microstructure is obtained by the classical evaluation process of the second law of thermodynamics applying the concept of Coleman and Noll (1963). In contrast to Svendsen (1999) no a priori assumption is made concerning the structure of the additional balance. It is remarkable that the resulting equation is comparable to the *balance of equilibrated forces* postulated by Goodman and Cowin (1972) and applied e.g. by Passman et al. (1984).

Compared to kinematically extended continuum models the formulation of the later models is more abstract with respect to the behavior of the microstructure, i.e. the micromotion is neither postulated nor restricted a priori. As the micromotion is only represented in a phenomenological (or homogenized) manner, this present kind of description can be interpreted as a kinematical model on an intermediate scale. In our context the micromotion, i.e. the kinematics of the polymer chains are rather complicated to describe and unknown in detail. From polymer literature it is just known, that the entanglement density of the polymer chains decreases near the surfaces (see e.g. Lee and Wool, 2001). But on the other hand it is well-known from experiments that the overall isothermal behavior of the polymeric bulk material differs from the behavior on the interphases (see e.g. Bockenheimer, 2003). It is also known, that the glass temperature in the interphase is not identical to the glass temperature of the bulk material. All these effects motivate us to introduce a scalar valued order parameter describing the influence of the boundaries on the microstructural behavior, i.e. the influence of the boundaries on the dynamics of the polymer chains is taken into account in a homogenized sense. Thus, the flux of the microstrucural field, which is a scalar valued force conjugated to the order parameter, can—as well as the scalar-valued order parameter itself—be described at the boundary.

The paper is organized as follows: After formulating the (standard) kinematical behavior, we present the governing classical balance equations and the extended balance of energy. Following the concept of Coleman and Noll (1963) we obtain restrictions for our constitutive equations and as an additional result we obtain the local form of the balance equation concerning the behavior of the microstructure. Next, we make further constitutive assumptions, which reduce our model to isothermal processes without phase transformations. In the forthcoming second part of this work, we consider the fully coupled problem.

[1] We do not claim to give a bibliographical overview of the historical development of extended continua. We refer the interested reader to the work of Truesdell (1966) and Capriz (1980, Appendix) where some remarks to the history are given and further references can be found.

In the last chapter we investigate a coupled two-field Galerkin-type finite element formulation for the governing (initial) boundary value problem for the displacement field $\mathbf{u}(\mathbf{x},t)$ and the additional field $\kappa(\mathbf{x},t)$ describing the microstructure. As a result of our investigations, we are able to describe boundary conditions for our additional field equation. Thus it is possible to investigate Dirichlet- and Neumann-type boundary conditions for the behavior on the microscale. Depending on the boundary conditions, we obtain either a stiff or a weak boundary layer with respect to the bulk material. As a consequence we compare effective moduli of our models with classical continua and explain the size effect under shear and tension.

2. Kinematical relations

The position vector of the center of mass of a microstructural element is given by $\mathbf{X}$ in the reference configuration and by $\mathbf{x}$ in the current configuration. If the microstructure does not change with respect to its center of mass, see Fig. 1, we are able to split the motion function into a macro- and micromotion. In the following, the effects according to the micromotion are described only by the abstract order parameter κ, where the macroscopic function of motion of the material point P is given as

$$\mathbf{x} = \boldsymbol{\chi}(\mathbf{X},t), \quad \mathbf{X} = \boldsymbol{\chi}^{-1}(\mathbf{x},t). \tag{1}$$

The deformation gradient $\mathbf{F}(\mathbf{X},t)$ is given as

$$\mathbf{F}(\mathbf{X},t) = \operatorname{Grad}\boldsymbol{\chi}(\mathbf{X},t), \quad \det\mathbf{F} > 0, \tag{2}$$

where $\operatorname{Grad}(\Diamond) := \partial(\Diamond)/\partial\mathbf{X}$ is the material gradient operator with respect to the initial or reference position $\mathbf{X}$. According to the usual definitions, the strain tensors are defined in terms of $\mathbf{F}$, e.g. the Green–Lagrangean strain tensor $\mathbf{E}$ is given by

$$\mathbf{E} := \frac{1}{2}(\mathbf{F}^{\mathrm{T}}\cdot\mathbf{F} - \mathbf{I}). \tag{3}$$

Within a standard Lagrangean setting the material time derivatives are defined as usual as

$$\dot{\mathbf{x}} = \mathbf{v} = \frac{\partial\boldsymbol{\chi}(\mathbf{X},t)}{\partial t} \quad \text{and} \quad \ddot{\mathbf{x}} = \dot{\mathbf{v}} = \mathbf{a} = \frac{\partial^2\boldsymbol{\chi}(\mathbf{X},t)}{\partial t}. \tag{4}$$

The introduction of the order parameter κ to describe the present microstructure is closely related to the description of materials with spherical voids, where the micromotion is related to a dilatation of the material points. In the context of materials with voids this is equivalent to a macrostructural description applying the concept of volume fractions. An equivalent kind of physical interpretation of the microstructural behavior

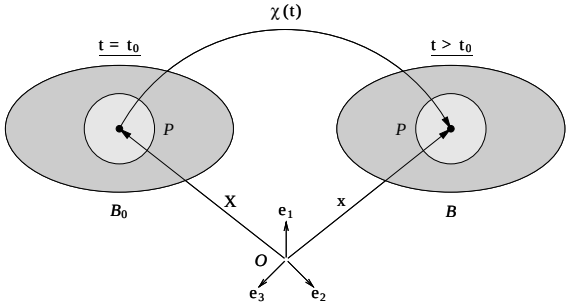

Fig. 1. Macroscopic motion function.

and further descriptions within continuum-based models is traced back to Goodman and Cowin (1972) and can also be found in the work of Lakes (1995).

3. General micro- and macroscopic balance equations

The extended balance of energy for the present type of continua with microstructure is given in the classical form

$$\frac{\mathrm{d}}{\mathrm{d}t}(E+K) = W + Q, \tag{5}$$

where E is the internal and K the kinetic energy, respectively. The mechanical power is associated with W while Q is the power of thermal sources and fluxes. In the context of continua with microstructures the kinetic energy and the mechanical power depend on an additional microstructural part, thus $K = K^{\mathrm{macro}} + K^{\mathrm{micro}}$ and $W = W^{\mathrm{macro}} + W^{\mathrm{micro}}$. We remark, that the assumed additive decomposition of the kinetic energy and the mechanical work is a more or less mathematical concept and related to very simple kinematical behavior of the microstructure or a phenomenological description of its behavior, see Fig. 1. If a more complex microstructural behavior is a priori known in more detail, a micro–macro coupling term has to be taken into account additionally (see e.g. Mindlin, 1964, Section 2).

Indeed the internal energy is given by

$$E = \int_B \rho\varepsilon \,\mathrm{d}v. \tag{6}$$

For the kinetic energy we assume [2]

$$K = K^{\mathrm{macro}} + K^{\mathrm{micro}} := \int_B \left(\frac{1}{2}\rho\,\dot{\mathbf{x}}\cdot\dot{\mathbf{x}} + \frac{1}{2}k\rho\dot{\kappa}\dot{\kappa}\right)\mathrm{d}v. \tag{7}$$

The (standard) first term is associated with the kinetic energy of the macroscopic motion, where the second term is the independent microscopic kinetic energy. [3] The thermal energy is given in the standard way as

$$Q = \int_B \rho r \,\mathrm{d}v + \int_{\partial B} q \,\mathrm{d}a = \int_B \rho r \,\mathrm{d}v - \int_{\partial B} \mathbf{q}\cdot\mathbf{n}\,\mathrm{d}a, \tag{8}$$

where r is the heat supply and $\mathbf{q}$ the heat flux. The outward normal is given by $\mathbf{n}$. The mechanical power is represented by its macro- and microscopic parts

$$W = W^{\mathrm{macro}} + W^{\mathrm{micro}} := \int_B \left(\rho\mathbf{b}\cdot\dot{\mathbf{x}} + \rho g\dot{\kappa}\right)\mathrm{d}v + \int_{\partial B}\left(\mathbf{t}\cdot\dot{\mathbf{x}} + s\dot{\kappa}\right)\mathrm{d}a. \tag{9}$$

Of course, we have applied a Cauchy theorem in the form $\mathbf{T}\cdot\mathbf{n} = \mathbf{t}$ for the classical second order macroscopic Cauchy stress tensor $\mathbf{T}$ and also for the first-order microscopic stresses $\mathbf{S}\cdot\mathbf{n} = s$. For the heat flux we have applied Stokes' heat flux theorem $-\mathbf{q}\cdot\mathbf{n} = q$. Furthermore, $\mathbf{b}$ are the macroscopic vector-valued and g the microscopic scalar-valued body forces.

[2] Conceptionally, vector- and tensor-valued quantities (...) which are describing the (affine) microstructure can be added in this context. Here, we neglect them for reasons of simplicity.

[3] Here we follow the proposal of Capriz and Podio-Guidugli (1983), where $k\rho$ is associated with the microinertia. From a physical point of view the microscopic kinetic energy could be the independent energy of the motion in a RVE under consideration with respect to e.g. molecular forces.

Assuming sufficient regularity of the field variables, the local form of the balance of energy is given by

$$\left(\rho\varepsilon+\frac{1}{2}\rho\dot{\mathbf{x}}\cdot\dot{\mathbf{x}}+\frac{1}{2}\rho k\dot{\kappa}\dot{\kappa}\right)^{\cdot}+\left(\rho\varepsilon+\frac{1}{2}\rho\dot{\mathbf{x}}\cdot\dot{\mathbf{x}}+\frac{1}{2}\rho k\dot{\kappa}\dot{\kappa}\right)\operatorname{div}\dot{\mathbf{x}}$$
$$=\operatorname{div}(\mathbf{T}^{\mathrm{T}}\cdot\dot{\mathbf{x}})+\operatorname{div}(\mathbf{S}\dot{\kappa})-\operatorname{div}\mathbf{q}+\rho\mathbf{b}\cdot\dot{\mathbf{x}}+\rho g\dot{\kappa}+\rho r. \tag{10}$$

Applying invariance requirements to the balance of energy the local balance equations (mass balance and balance of momentum) are obtained as a result. In our context, we obtain from invariance analyses just the balance equations of a classical continuum theory which are now locally given in the spatial setting:

- Balance of mass

$$\dot{\rho}+\rho\operatorname{div}\dot{\mathbf{x}}=0. \tag{11}$$

- Balance of momentum

$$\rho\ddot{\mathbf{x}}=\operatorname{div}\mathbf{T}+\rho\mathbf{b}. \tag{12}$$

- Balance of moment of momentum (Boltzmann-assumption)

$$\mathbf{T}^{\mathrm{T}}=\mathbf{T}. \tag{13}$$

In addition, higher order balance equations are obtainable for affine microstructures, i.e. for vectorial or tensorial extensions of the microscopic kinetic energy K^{micro} and the microscopic external power W^{micro}, see (7) and (9), e.g. (Capriz et al., 1982).

3.1. Thermodynamical considerations

After evaluating the invariance requirements (change of observer), the set of governing equations has to be enriched by constitutive equations which have to fulfill the second law of thermodynamics. Thus, the balance of entropy is now written in the local form

$$(\rho\eta)^{\cdot}+\rho\eta\operatorname{div}\dot{\mathbf{x}}=\operatorname{div}\boldsymbol{\varphi}_{\eta}+\rho s_{\eta}+\hat{\eta}. \tag{14}$$

In contrast to Eqs. (11)–(13) the balance of entropy restricts the direction of the thermodynamical process, i.e. it requires the entropy production during the process to be always positive $\hat{\eta}\geqslant 0$. In our contribution—differing from the work of Svendsen (1999)—we evaluate the balance of entropy following the concept of Coleman and Noll (1963). In contrast to the more general evaluation concept of Müller (1985) and Liu (1972), where the lower order balance equations are added to the balance of entropy via Lagrangean multipliers, we have to make several constitutive assumptions a priori. The consequences of the Coleman-Noll procedure are on the one hand constitutive equations with sharper restrictions compared to the more general results of the Müller–Liu approach. On the other hand, we do not have to know the structure of further "balance equations" *before* evaluating the entropy balance. This means that in the present contribution additional balance equations are *automatically* dropped out of the evaluation process.

We constitutively assume for the entropy flux $\boldsymbol{\varphi}_{\eta}$ and the entropy supply s_{η}

$$\boldsymbol{\varphi}_{\eta}=\frac{\mathbf{q}}{\Theta}\quad\text{and}\quad s_{\eta}=\frac{r}{\Theta} \tag{15}$$

and also for the Helmholtz free energy Ψ

$$\Psi=\varepsilon-\eta\Theta. \tag{16}$$

Using the lower order mass balance equation (11) and the balance of momentum equation (12) the balance of energy can be reduced to the balance of *internal energy* [4]

$$\rho\dot{\varepsilon}+\frac{1}{2}\rho\dot{k}\dot{\kappa}\dot{\kappa}+\rho k\dot{\kappa}\ddot{\kappa}=\mathbf{T}:\operatorname{grad}\dot{\mathbf{x}}+\operatorname{div}(\mathbf{S}\dot{\kappa})-\operatorname{div}\mathbf{q}+\rho g\dot{\kappa}+\rho r, \tag{17}$$

which now contains macroscopic as well as microscopic contributions. Inserting the assumptions, Eqs. (15) and (16), the balance of entropy can be reformulated

$$\rho\dot{\varepsilon}-\rho\eta\dot{\Theta}-\rho\dot{\Psi}-\operatorname{div}\mathbf{q}+\Theta\mathbf{q}\cdot\operatorname{grad}\frac{1}{\Theta}-\rho r\geqslant 0. \tag{18}$$

The Clausius–Duhem inequality is obtained, if $\rho\dot{\varepsilon}$ is finally eliminated with the aid of Eq. (17) yielding

$$\frac{1}{2}\rho\dot{k}\dot{\kappa}\dot{\kappa}-\rho k\dot{\kappa}\ddot{\kappa}+\mathbf{T}:\operatorname{grad}\dot{\mathbf{x}}+\operatorname{div}(\mathbf{S}\dot{\kappa})+\rho g\dot{\kappa}-\rho\dot{\Psi}-\rho\eta\dot{\Theta}+\Theta\mathbf{q}\cdot\operatorname{grad}\frac{1}{\Theta}\geqslant 0. \tag{19}$$

The thermodynamical process variables for simple and reversible solid materials are constitutively chosen as

$$\mathscr{S}=\mathscr{S}(\Theta,\operatorname{grad}\Theta,\mathbf{E},\kappa,\operatorname{grad}\kappa) \tag{20}$$

thus, according to the concept of equipresence (Truesdell and Toupin, 1960, Section 293), the following dependencies are assumed:

$$\begin{aligned}
&\Psi=\Psi(\Theta,\operatorname{grad}\Theta,\mathbf{E},\kappa,\operatorname{grad}\kappa),\\
&\mathbf{T}=\mathbf{T}(\Theta,\operatorname{grad}\Theta,\mathbf{E},\kappa,\operatorname{grad}\kappa),\\
&\mathbf{S}=\mathbf{S}(\Theta,\operatorname{grad}\Theta,\mathbf{E},\kappa,\operatorname{grad}\kappa),\\
&k=k(\Theta,\operatorname{grad}\Theta,\mathbf{E},\kappa,\operatorname{grad}\kappa),\\
&\mathbf{q}=\mathbf{q}(\Theta,\operatorname{grad}\Theta,\mathbf{E},\kappa,\operatorname{grad}\kappa).
\end{aligned} \tag{21}$$

Additionally, the set of response functions $\mathscr{R}$ which has to be determined is given by

$$\mathscr{R}=\mathscr{R}(\Psi,\mathbf{T},\mathbf{S},k,\mathbf{q}). \tag{22}$$

Therefore, the material time derivative of an arbitrary response function $\dot{(\Diamond)}$ is computed as

$$\dot{(\Diamond)}=\frac{\partial(\Diamond)}{\partial\Theta}\dot{\Theta}+\frac{\partial(\Diamond)}{\partial\operatorname{grad}\Theta}\cdot\operatorname{grad}\dot{\Theta}+\frac{\partial(\Diamond)}{\partial\mathbf{E}}:\dot{\mathbf{E}}+\frac{\partial(\Diamond)}{\partial\kappa}\dot{\kappa}+\frac{\partial(\Diamond)}{\partial\operatorname{grad}\kappa}\cdot\operatorname{grad}\dot{\kappa}. \tag{23}$$

Applying the standard arguments of evaluation of the entropy balance leads to the following scalar-, vector- and tensor-valued consequences

$$\dot{\Theta}:\quad 0=\eta+\frac{\partial\Psi}{\partial\Theta}+\frac{1}{2}\dot{\kappa}\dot{\kappa}\frac{\partial k}{\partial\Theta}, \tag{24}$$

$$\operatorname{grad}\dot{\Theta}:\quad \mathbf{0}=\frac{\partial\Psi}{\partial\operatorname{grad}\Theta}+\frac{1}{2}\dot{\kappa}\dot{\kappa}\frac{\partial k}{\partial\operatorname{grad}\Theta}, \tag{25}$$

$$\dot{\mathbf{E}}:\quad \mathbf{0}=\mathbf{T}-\rho\frac{\partial\Psi}{\partial\mathbf{E}}-\frac{1}{2}\rho\dot{\kappa}\dot{\kappa}\frac{\partial k}{\partial\mathbf{E}}, \tag{26}$$

[4] In this concept, we enhance the classical set of balance equations by an extended balance of energy with respect to the governing microstructure. Thus the coupling of the macroscopical and microscopical behavior is observed in the balance of internal energy and the resulting equations of the thermodynamical evaluation process only.

$$\operatorname{grad}\dot{\kappa} \quad \mathbf{0} = \mathbf{S} - \rho\frac{\partial \Psi}{\partial \operatorname{grad}\kappa} - \frac{1}{2}\rho\dot{\kappa}\dot{\kappa}\frac{\partial k}{\partial \operatorname{grad}\kappa}, \tag{27}$$

$$\dot{\kappa}: \quad 0 = \frac{1}{2}\rho\dot{\kappa}\dot{\kappa}\frac{\partial k}{\partial \kappa} + \rho k\ddot{\kappa} - \rho g + \rho\frac{\partial \Psi}{\partial \kappa} - \operatorname{div}\mathbf{S}, \tag{28}$$

and the dissipation inequality (which leads to the well known Fourier's law)

$$\mathbf{q}\cdot\operatorname{grad}\frac{1}{\Theta} \geqslant 0. \tag{29}$$

It should be remarked that on the one hand expressions which are comparable to Eq. (28) can be found e.g. in the work of (Goodman and Cowin, 1972), where the additional balance equation is named *balance of equilibrated forces* and describes the behavior of the microstructure of a granular material, i.e. the void space between the grains. On the other hand, equations of type (28) are applied in the context of porous materials (see e.g. Passman et al., 1984), where the scalar-valued microforce s is conjugated to the volume fractions, i.e. the order parameter is identified as the volume fractions $\kappa := n^{\alpha} = \mathrm{d}V^{\alpha}/\mathrm{d}V$ of a single constituent φ^{α}.

4. A small-strain isothermal model with scalar order parameter

In the present section we precise our constitutive assumptions for an abstract model material, which shows the mentioned "weaker" boundary layer effect. For the case of simplicity, we restrict ourselves in this first part of our work on the quasi-static, isothermal process, which is equivalent to a nonevolving interphase. In addition, it has to be remarked that the restriction to quadratic terms in the present free energy confines the model to small deformations. In a forthcoming paper, the theory and numerics are extended to the thermo-mechanically coupled problem at finite deformations. Thus, the evolution of the interphase can also be captured. Furthermore, the microinertia k is thought to be constant during the process, i.e. $k = \text{const.}$ and $\partial k/\partial a = 0, \forall a \in \mathscr{S}$. Thus, the Helmholtz free energy $\Psi = \Psi(\mathbf{E}, \kappa, \operatorname{grad}\kappa)$ is assumed to have the following format:

$$\begin{aligned}\rho\Psi = {} & \mu\mathbf{E}:\mathbf{E} + \frac{1}{2}\lambda(\mathbf{E}:\mathbf{I})^2 + \frac{1}{2}\alpha(\kappa-\kappa_0)^2 + \frac{1}{2}\beta(\operatorname{grad}\kappa)^2 + \mu[\exp(\gamma(\kappa-\kappa_0)-1)]\mathbf{E}:\mathbf{E} \\ & + \frac{1}{2}\lambda[\exp(\phi(\kappa-\kappa_0)-1)](\mathbf{E}:\mathbf{I})^2.\end{aligned} \tag{30}$$

The macroscopic Cauchy stresses $\mathbf{T}$, see Eq. (26), are defined as

$$\mathbf{T} = \rho\frac{\partial \Psi}{\partial \mathbf{E}} = 2\mu[\exp(\gamma(\kappa-\kappa_0))]\mathbf{E} + \lambda[\exp(\phi(\kappa-\kappa_0))](\mathbf{E}:\mathbf{I})\mathbf{I}. \tag{31}$$

Furthermore the microscopic (scalar) forces p are calculated from Eq. (28) [5]

$$p := \rho\frac{\partial \Psi}{\partial \kappa} = \alpha(\kappa-\kappa_0) + \mu\gamma[\exp(\gamma(\kappa-\kappa_0))]\mathbf{E}:\mathbf{E} + \frac{1}{2}\lambda\phi[\exp(\phi(\kappa-\kappa_0))](\mathbf{E}:\mathbf{I})^2 \tag{32}$$

[5] The scalar microscopic force p can also be interpreted as a *configurational pressure* because of its volumetrical characteristic. Generally speaking, a configurational pressure is the driving force according to the change in volume fractions of the various phases of the microstructure and can also be found in works on phase transition, e.g. in granular mixtures (see Kirchner and Hutter, 2003).

and the microscopic stresses $\mathbf{S}$, see Eq. (27), are obtained as

$$\mathbf{S} = \rho \frac{\partial \Psi}{\partial \operatorname{grad} \kappa} = \beta \operatorname{grad} \kappa. \tag{33}$$

Recapitulating all this, the overall micro- and macroscopic material parameters $\mathscr{M}$ are given for the present model as the set

$$\mathscr{M} = \{\mu, \lambda, \alpha, \beta, \gamma, \phi, \kappa_0\} \tag{34}$$

where the first two entries μ, λ are the classical Lamé parameters according to the macroscopical behavior. The latter parameters $\alpha, \beta, \gamma, \phi, \kappa_0$ describe the microscopical behavior and the interaction between the micro- and macroscale, respectively.

Special attention is directed to Eq. (32), which includes the definition of the microscopic force p. In contrast to the decoupled microscopic stress $\mathbf{S}$, the microscopic force p is coupled to the macroscopic part. On the other hand, the macroscopic stresses $\mathbf{T}$ are related to the microstructure.

Completing the set of governing equations, it is shown that the set of balance equations are explicitely decoupled a priori, related to the assumption of decoupled kinetic energy. All the micro- and macroscopic coupling effects are later on obtained from thermodynamical requirements with respect to certain constitutive assumptions.

5. Finite element implementation and numerical examples

5.1. Finite element discretization

After formulating the governing set of balance and constitutive equations we are able to solve the quasi-static set of coupled equations applying a mixed Bubnov–Galerkin finite element formulation. The set of governing equations is given in a weak form by the balance of momentum, Eq. (12), and the weak form of the microscopic momentum balance, Eq. (28),

$$\int_B \mathbf{T} : \operatorname{grad} \delta\mathbf{u} \, \mathrm{d}v = \int_{\partial B} \mathbf{t} \cdot \delta\mathbf{u} \, da + \int_B \rho\mathbf{b} \cdot \delta\mathbf{u} \, \mathrm{d}v, \tag{35}$$

$$\int_B \mathbf{S} \cdot \operatorname{grad} \delta\kappa \, \mathrm{d}v = \int_{\partial B} s\,\delta\kappa \, \mathrm{d}a + \int_B (\rho g + p)\,\delta\kappa \, \mathrm{d}v, \tag{36}$$

with the test functions $\delta\mathbf{u} \in \mathscr{V}^{\mathbf{u}}$, and $\mathscr{V}^{\mathbf{u}} := \{\delta\mathbf{u} \in \mathscr{H}^1(\Omega \to \mathscr{B}), \delta\mathbf{u}|^{\mathbf{u}}_{\Gamma_D} = 0\}$ and the scalar-valued test function $\delta\kappa \in \mathscr{V}^{\kappa}$ with $\mathscr{V}^{\kappa} := \{\delta\kappa \in \mathscr{H}^1(\Omega \to \mathscr{B}), \delta\kappa|^{\kappa}_{\Gamma_D} = 0\}$. In addition, Ω is the domain of the body $\mathscr{B}$. The boundary $\partial\Omega$ of the domain is split into a Dirichlet part $\Gamma^{\mathfrak{b}}_D \subset \partial\Omega$ and a Neumann part $\Gamma^{\mathfrak{b}}_N \subset \partial\Omega$, with $\Gamma^{\mathfrak{b}}_D \cup \Gamma^{\mathfrak{b}}_N = \partial\Omega, \forall \mathfrak{b} \in \{\mathbf{u}, \kappa\}$. The displacements $\mathbf{u}$ and the order parameter κ are discretized by standard ansatz functions $\mathbf{u}_h \in \mathscr{U}^{\mathbf{u}}_h \subset \mathscr{U}^{\mathbf{u}}$ and $\kappa_h \in \mathscr{U}^{\kappa}_h \subset \mathscr{U}^{\kappa}$. In the present numerical examples we use three node triangular Q1P1, six node Q2P2 as well as six node Q2P1 elements, i.e. quadratical ansatz functions for the displacements and linear ansatz functions for the order parameter, equivalent to a Taylor–Hood formulation which is known to fulfill the Ladyzhenskaya–Babuška–Brezzi (LBB) condition (see e.g. Brenner and Scott, 1994). As can be seen in Fig. 2, the Q1P1 and Q2P2 elements are more efficient than the Taylor–Hood element, which is indeed quite different from various other numerical discretization schemes for higher order continua, c.f. finite element formulations for Cosserat-continua. From our experiences, this effect could be explained by the lower coupling effect of the present model, which is only given in the constitutive equations and not in the kinematical quantities.

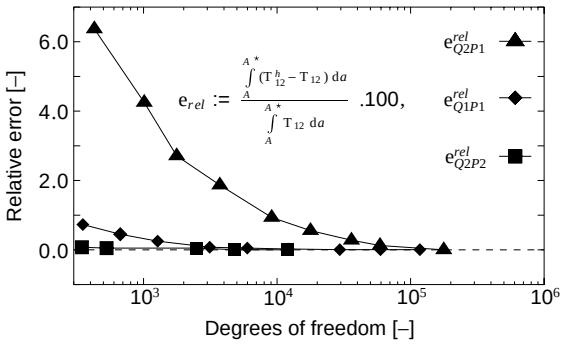

Fig. 2. Discretization error of a resulting force $Q = \int_A^{A^*} T_{12}\,da$.

Subsequently, the set of governing nonlinear partial differential equations is linearized and solved within a standard global Newton–Raphson iteration scheme. The governing set of equations is implemented in the finite element toolbox PANDAS (see Ehlers and Ellsiepen, 1998).

Numerical difficulties resulting from the steep gradients of the primary variables in the boundary layer zone are circumvented by simple mesh refinement techniques. Thus a heuristic error indicator is formulated for the coupled problem which traces back to the well-known gradient-based Z^2 error indicator for one-phase materials (c.f. Zienkiewicz and Zhu, 1987). Our investigation is related to an extension of this error indicator for multi-phase materials which was formulated by Ellsiepen (1999). Thus, the element-wise error indicator η_T^α for all finite elements $T \in \mathscr{T}$ is defined as:

$$\eta_T^{\mathbf{T}} := \|\overset{*}{\mathbf{T}} - \mathbf{T_h}\|_{\mathbf{T}}, \tag{37}$$

$$\eta_T^{\mathbf{S}} := \|\overset{*}{\mathbf{S}} - \mathbf{S_h}\|_{\mathbf{T}}, \tag{38}$$

where $\|\Diamond\|_T$ is the element-depending L_2-norm of the macro- and microstresses, respectively. The finite element solution is denoted with the index h. The smoothed stress fields $\overset{*}{\mathbf{T}}, \overset{*}{\mathbf{S}}$ are calculated in a post-processing step with the Superconvergent Patch Recovery (SPR) method, c.f. (Zienkiewicz and Zhu, 1992). Subsequently, a relative error measure $\xi_{\alpha,T}$ is formulated in the standard way

$$\xi_{\alpha,T} := \frac{\eta_T^\alpha}{\mathrm{TOL}_\alpha}, \quad \text{with } \alpha \in \{\mathbf{T}, \mathbf{S}\}, \tag{39}$$

which leads to overall local and global error measures $\xi_T(\mathbf{T}_h, \mathbf{S}_h)$ and $\xi(\mathbf{T}_h, \mathbf{S}_h)$

$$\xi_T := \left(\sum_\alpha C_\alpha \xi_{\alpha,T}^2 \right)^{1/2}, \quad \text{where } C_{\mathbf{T}} + C_{\mathbf{S}} = 1 \text{ and } \xi := \left(\sum_{T \in \mathscr{T}} \xi_T^2 \right)^{1/2} \tag{40}$$

with the weighting factors C_α.

5.2. Example 1: Shear test

In the first numerical example we investigate a shear experiment as shown in Fig. 3. This kind of experiment can also be analyzed in the laboratory, where the displacement boundary conditions $u_1 = \eta(t)\bar{u}_1$ are related to a (stiff) load plate which is bonded at the top and bottom of the specimen. Thus, simple shear effects are only expected in the mid of the specimen, where all the edge effects, resulting from the boundary effects of the free boundary but also from the Dirichlet boundary conditions of the order parameter, are

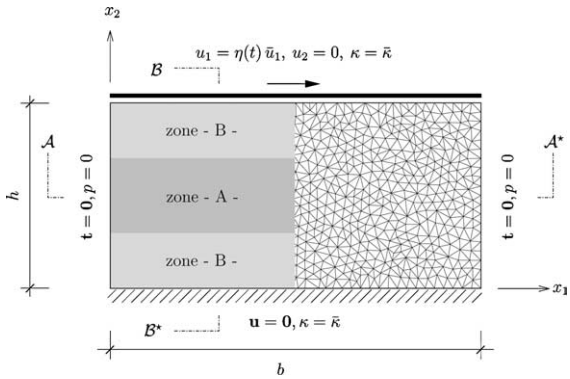

Fig. 3. Shear test—infinite long strip under shear deformation.

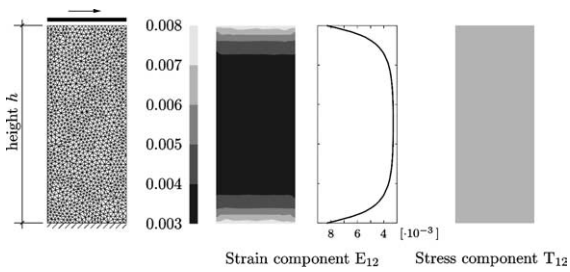

Fig. 4. Shear test—response of macroscopic quantities.

vanishing. Therefore, only results in a small strip in the mid of the specimen are shown in the present numerical experiments. The set of material parameters $\mathscr{M}$ for the considered artificial material is assumed as follows:

μ [MPa]	λ [MPa]	α [MPa]	β [MPa]	γ []	ϕ []	κ_0 []
10 000.0	5 000.0	2.0	1 000.0	1.0	1.0	1.0

The numerical investigation is analyzed within an adaptive finite element procedure, applying Q2P2 elements. Therefore, the initial mesh of the problem is shown in Fig. 4. According to the specified shear example in Fig. 3, we prescribe Dirichlet boundary conditions at the top and bottom for the displacements $\mathbf{u}$ and the order parameter κ, respectively. The prescribed boundary conditions $\kappa = \bar{\kappa}$ of the order parameter are motivated by advanced characterization methods giving insight into the material behavior of the polymer at a free boundary or at the interphase to e.g. aluminum alloys (see Bockenheimer, 2003).

On the other hand, the behavior of the bulk material is prescribed with the equilibrium parameter κ_0. [6] In our examples $\bar{\kappa}$ is chosen in such a way that it models weak boundary layer effects; the width of the boundary layer is small, according to the material parameter α, compared to the height h of the specimen. The numerical results show the expected behavior for a small shear angle $\gamma = u_1/h = 0.01$. On the one hand,

[6] We assume here, that the microstructural configuration at thermodynamical equilibrium is known at the boundaries. This means, that the characteristic glass temperature, the entanglement density, the chemical decomposition or various other quantities of the polymer are well-known at the interphase to other materials as well as the behavior of the polymer bulk.

the shear strains E_{12} near the boundary (zone B) are large compared to those of the bulk, see Fig. 4, due to the coupling effects of the micro- and macroscopic quantities in the constitutive equations. On the other hand, the macroscopic equilibrium is well captured, as is shown in the homogeneous distribution of the shear stresses T_{12}, see Fig. 4. The behavior of the displacements and the microstructure of the polymer are shown in Fig. 5. Again, it can be observed that the boundary layer effect is captured by the order parameter κ due to the prescribed boundary conditions. With respect to the set of material parameters, κ vanishes at the boundary and converges to the equilibrium parameter κ_0 in the bulk. According to the gradient of the order parameter, the microstress S_2 is developed inside the domain.

Next, we are interested in the size effect of the material. Thus, we vary the height h of the specimen, keeping the set of material parameters constant. As a consequence, the boundary layer gets thinner and thinner with respect to the specimen size by increasing the height h. The overall effect from an quantitative point of view can be captured by the effective shear modulus G^{eff}. This secant modulus is calculated by applying the same shear angle $\gamma = u_1/h$ to different specimen heights h. Thereafter, the effective modulus is calculated as the secant $G^{\text{eff}} = T_{12}/\gamma$. As it can be seen in Fig. 6, the effective shear modulus converges to a minimum quantity. In this case the microstructure dominates the global behavior. Otherwise it converges to a maximum quantity with dominating bulk material behavior. It has to be remarked, that the overall problem is energy driven, which results in maximum moduli which are not directly comparable to the classical moduli of elasticity because of the portion of the microscopic free energy.

The consequence of the adaptive mesh-refinement, c.f. Fig. 7, are well-analyzed gradients in the boundary layer and thus more effective overall finite element calculations. An example of the calculation of the order parameter within an adaptive finite element procedure is presented in Fig. 8. In the analyzed example the material parameter α, c.f. Eq. (30) and (32), was chosen to be rather small which results in a

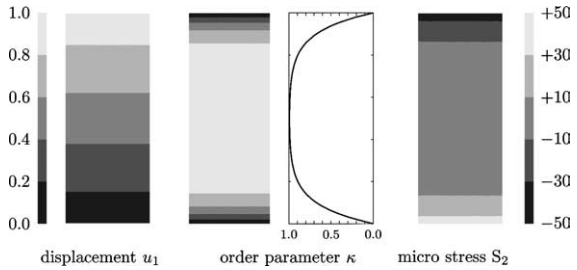

Fig. 5. Shear test—response of microscopic quantities and displacement.

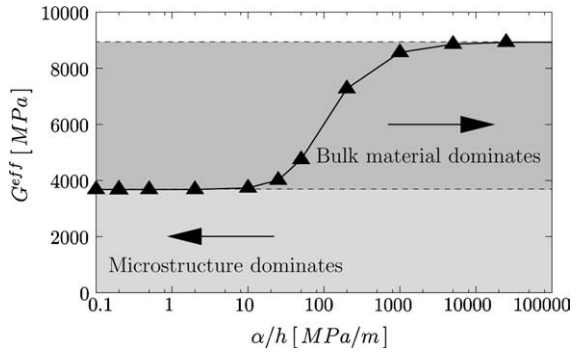

Fig. 6. Effective shear modulus G^{eff}.

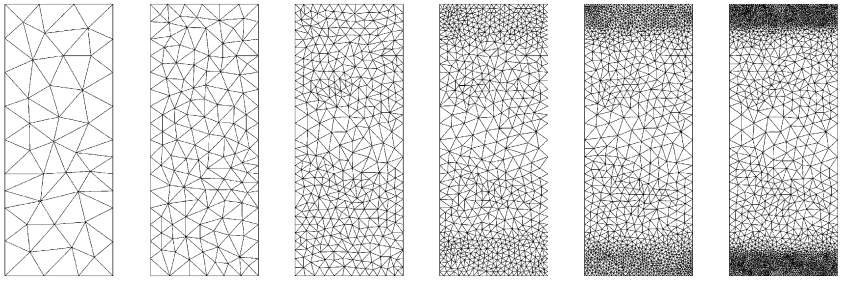

Fig. 7. Adaptive refined meshes for the shear test.

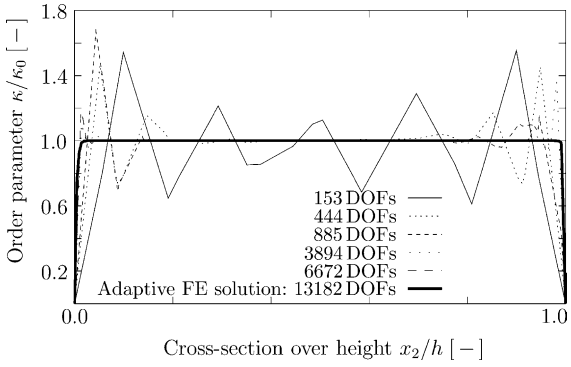

Fig. 8. Adaptive solution of order parameter κ in a shear test (cross-section $B - B^{\star}$).

narrow boundary layer. Thus, difficulties in the numerical calculations occur, resulting in oscillations near the observed boundary layer. As it can be observed in Fig. 8, the quality of the numerical calculation can be well improved by adaptive remeshing techniques, where only the domain of the boundary is refined.

5.3. Example 2: tension test

In the second example we investigate a tension test. Again we apply Dirichlet boundary conditions for the displacements ($u_2 = \bar{u}_2$ and $\kappa = \bar{\kappa}$) at the top and bottom of the specimen according to Fig. 3. As can be see in Fig. 9 and Fig. 10 the qualitative behavior of the macroscopic components, e.g. $E_{22}, T_{22}, u_2, \kappa$ and S_2, of the specimen is comparable to the first (shear) experiment. As seen before, a weak boundary layer effect is observed according to the applied set of material parameters. Again, we are interesting in the size effect of the material under tension. Thus, we calculate an effective secant Young's modulus comparable to the (shear) modulus of the first example. We therefore calculate again various problems with different height h keeping the set of material data constant. The applied strain E_{22} is constant in all experiments, i.e. $E_{22} = \bar{u}_2/h = 0.01$. As can be seen in Fig. 11 the effective Young's modulus converges again to a limit quantity representing the bulk behavior at infinite height h and another limit quantity representing just the microstructure for $h \to 0$.

Remark. According to the chosen boundary data of the order parameter $\kappa = \bar{\kappa}$ and equilibrium data κ_0 we are also able to describe a stiff boundary layer effect. As a stiff boundary layer effect is quite natural in

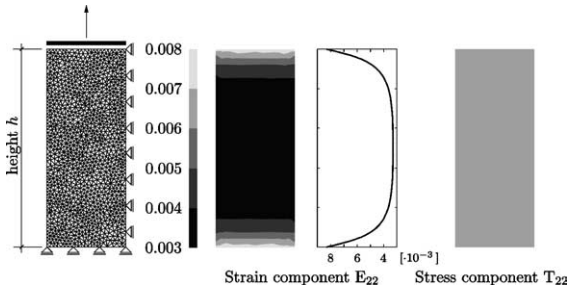

Fig. 9. Tension test—response of macroscopic quantities.

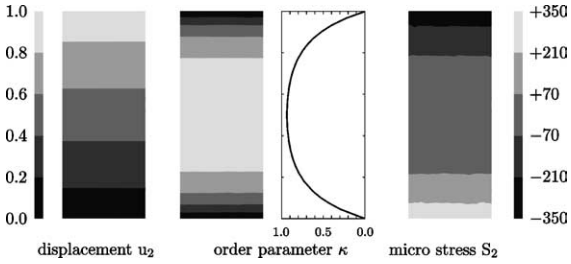

Fig. 10. Tension test—response of microscopic quantities and displacement.

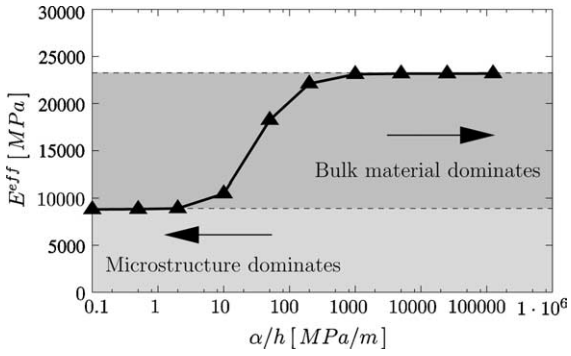

Fig. 11. Effective young's modulus E^{eff}.

higher order continua with enhanced kinematics, [7] we have not investigated such experiments in further details in this work.

[7] We want to mention the size effect in cellular materials, e.g. foams, which are modeled by Cosserat continua (see Onck et al., 2001 or Diebels and Steeb, 2002). Thus the total rotations of the model are restricted at the top and bottom in the shear experiment. Therefore, couple stresses occur in a boundary layer near the top and bottom of the specimen. The effective shear modulus of the foam is larger compared with classical continua. Of course, in the tension experiment, no size effect is noticed applying a Cosserat model.

6. Conclusions and discussion

In the present work we have developed an extended continuum model to describe the behavior of thin polymeric films with respect to experimentally observed boundary layer effects. It was shown that the known *weak boundary effect* can be captured very well within representative numerical examples for an artificial model material. Furthermore the resulting size effect of the material is captured under shear and tension.

The present extended continuum-based model captures the development of this weaker zone within a thermo-mechanical coupled model. In this first approach the isothermal case is considered constitutively and numerically. Thus, the microstructure is prescribed by the enhanced microscopic boundary condition, the equilibrium part of the order parameter and the full set of microstructural material parameters. In the full thermo-mechanical coupled model evolving microstructures can also be described. More sophisticated constitutive equations and numerical experiments will verify this in a forthcoming paper. As experimental data of this kind of problems within thin polymeric films with respect to the analyzed size effect are very rare, we also want to investigate experiments for these problems in the future. Thus, the set $\mathscr{M}$ of material parameters can also be identified numerically, e.g. by use of numerical parameter identification methods.

Acknowledgements

The authors thank Prof. Wulff Possart, Saarland University, for arousing their interest in the exciting research field of polymeric materials and for the stimulating discussions about applications and experiments of thin polymeric films.

References

Bockenheimer, C., 2003. Epoxid und Aluminium im Kleberverbund nach mechanischer Vorbehandlung und Alterung. Ph.D. Thesis, Saarland University.

Brenner, S., Scott, L., 1994. The Mathematical Theory of Finite Element Methods. Texts in Applied Mathematics. Springer-Verlag, Berlin.

Capriz, G., 1980. Continua with microstructures. In: Springer Tracts in Natural Philosophy, vol. 35. Springer, New York.

Capriz, G., Podio-Guidugli, P., 1983. Structured continua from a Lagrangian point of view. Ann. Mater. Pura Appl. 135, 1–25.

Capriz, G., Podio-Guidugli, P., Williams, W., 1982. On balance equations for materials with affine structure. Meccanica 17, 80–84.

Coleman, B., Noll, W., 1963. The thermodynamics of elastic materials with heat conduction and viscosity. Arch. Rat. Mech. Anal. 13, 167–178.

Cosserat, E., Cosserat, F., 1909. Théorie des corps déformables. A. Hermann et Fils, Paris.

Diebels, S., Steeb, H., 2002. The size effect in foams and its theoretical and numerical investigation. Proc. R. Soc. Lond. A 458, 2869–2883.

Ehlers, W., Ellsiepen, P., 1998. PANDAS: Ein FE-System zur Simulation von Sonderproblemen der Bodenmechanik. In: Wriggers, P., Meißner, U., Stein, E., Wunderlich, W. (Eds.), Finite Elemente in der Baupraxis: Modellierung, Berechnung und Konstruktion, Beiträge zur Tagung FEM '98 an der TU Darmstadt am 5. und 6. März 1998. Ernst & Sohn, Berlin, pp. 391–400.

Ellsiepen, P., 1999. Zeit-und Ortsadaptive Verfahren angewandt auf Mehrphasenprobleme poröser Medien. Ph.D. Thesis, Institute of Applied Mechanics (CE), Chair II, University of Stuttgart.

Eringen, C., 1999. Microcontinuum field theories. In: Foundations and Solids, vol. I. Springer-Verlag, Berlin.

Eringen, A., Suhubi, E., 1964. Nonlinear theory of simple micro-elastic solids—I. Int. J. Eng. Sci. 2, 189–203.

Frank, B., Gast, A., Russell, T., Brown, H., Hawker, C., 1996. Polymer mobility in thin films. Macromolecules 29, 6531–6534.

Goodman, M., Cowin, S., 1972. A continuum theory for granular materials. Arch. Rat. Mech. Anal. 44, 249–266.

Günther, W., 1958. Zur Statik und Kinematik des Cosseratschen Kontinuums. Abhandlungen der Braunschweigischen Wissenschaftlichen Gesellschaft 10, 195–213.

Kirchner, N., Hutter, K., 2003. Modelling particles size segregation in granular mixtures. In: Hutter, K., Kirchner, N. (Eds.), Dynamic response of granular and porous materials under large and catastrophic defomations. Springer-Verlag, Berlin.

Lakes, R., 1995. Experimental methods for study of Cosserat elastic solids and other generalized elastic continua. In: Mühlhaus, H. (Ed.), Continuum Methods for Materials with Microstructures. John Wiley and Sons, Chichester, pp. 1–25.

Lee, I., Wool, R., 2001. Thermodynamic analysis of polymer-solid adhesion: Sticker and receptor group effects. J. Polym. Sci., Part B: Polym. Phys. 40, 2343–2353.

Liu, I.-S., 1972. Method of Lagrangian multipliers for exploitation of the entropy principle. Arch. Rat. Mech. Anal. 46, 131–148.

Mindlin, R., 1964. Micro-structure in linear elasticity. Arch. Rat. Mech. Anal. 16, 51–78.

Mindlin, R., Tiersten, H., 1962. Effects of couple-stresses in linear elasticity. Arch. Rat. Mech. Anal. 11, 415–448.

Müller, I., 1985. Thermodynamics. Pitman, Boston.

Onck, P., Andrews, E., Gibson, L., 2001. Size effects in ductile cellular solids. Part II: experimental results. Int. J. Mech. Sci. 43, 701–713.

Passman, S., Nunziato, J., Walsh, E., 1984. A theory of multiphase mixtures. In: Truesdell, C. (Ed.), Rational Thermodynamics. Springer-Verlag, Berlin, pp. 286–325.

Svendsen, B., 1999. On the thermodynamics of thermoelastic materials with additional scalar degrees of freedom. Continuum Mech. Thermodyn. 4, 247–262.

Toney, M., Russell, T., Logan, J., Kikuchi, H., Sands, J., Kumar, S., 1995. Near-surface alignment of polymers in rubbed films. Nature 374, 709–711, doi:10.1038/374709a0.

Truesdell, C., 1966. Six lectures on modern natural philosophy. Springer-Verlag, Berlin.

Truesdell, C., Toupin, R., 1960. The classical field theories. In: Flügge, S. (Ed.), Handbuch der Physik, vol. III/1. Springer-Verlag, Berlin.

Šilhavý, M., 1997. The Mechanics and Thermodynamics of Continuous Media. Springer-Verlag, Berlin.

Zienkiewicz, O., Zhu, J., 1987. A simple error estimator and adaptive procedure for practical engineering analysis. Int. J. Numer. Meth. Eng. 24, 337–357.

Zienkiewicz, O., Zhu, J., 1992. The superconvergent patch recovery and *a posteriori* error estimates. Part 1: The recovery technique. Int. J. Numer. Meth. Eng. 33, 1331–1364.